Design of pseudo-mechanisms and multistable units for mechanical metamaterials

Singh, N.; Hecke, M.L. van

Note: To cite this publication please use the final published version (if applicable).

Design of Pseudo-Mechanisms and Multistable Units for Mechanical Metamaterials

Nitin Singh[1] and Martin van Hecke[1,2]

[1]*AMOLF, Science Park 104, 1098 XG Amsterdam, Netherlands*
[2]*Huygens-Kamerlingh Onnes Lab, Leiden University, PObox 9504, 2300 RA Leiden, Netherlands*

Mechanisms—collections of rigid elements coupled by perfect hinges which exhibit a zero-energy motion—motivate the design of a variety of mechanical metamaterials. We enlarge this design space by considering *pseudo-mechanisms*, collections of elastically coupled elements that exhibit motions with very low energy costs. We show that their geometric design generally is distinct from those of true mechanisms, thus opening up a large and virtually unexplored design space. We further extend this space by designing building blocks with bistable and tristable energy landscapes, realize these by 3D printing, and show how these form unit cells for multistable metamaterials.

A mechanism is a collection of flexibly linked, rigid elements which exhibits a zero-energy motion. Mechanisms play a foundational role in the physics of jammed media and spring networks [1–7], and are central in mechanical engineering, where they underlie the design of robotic devices such as grippers [8,9]. Imperfect mechanisms, based on distorted geometries [10–13], extra bonds or connections [1–7], or nonideal hinges [14] frequently occur, and these exhibit soft modes similar to the zero energy motions of the underlying mechanism. In particular, mechanism-based metamaterials borrow the geometric design of mechanisms but replace the hinges by slender, flexible parts which connect stiffer elements, such that the soft modes of the metamaterial are similar to the free motion of the underlying mechanism. External forces easily excite these soft modes, and as the mechanism-derived soft modes can be very different from those of ordinary elastic modes, exotic properties may emerge [15], including negative response parameters [16–18], shape-morphing [19–22], topological polarization [23–26], programmability and multistability [10,11,27–29] and (self-)folding [10–12,20,24,29–35].

However, as mechanism-based metamaterials do not have true zero modes [14,15], the design of a flexible metamaterial does not require an underlying true zero-energy mechanism. This suggests one to consider *pseudo-mechanisms* (PMs), which we define as collections of flexibly coupled rigid elements that exhibit motions with (very) low energy costs.

Here we show that PMs are widespread, by constructing quadrilateral based PMs by use of particle swarm optimization. Our central finding is that most PMs are geometrically very distinct from true mechanisms; most PMs are not simply perturbed mechanisms, but PMs permeate the design space very far away from the true mechanism subspace. We extend our search techniques to obtain multistable units [27], and bring these to life using 3D printing. Finally, we show how to tile our unit cells to obtain complex periodic metamaterials. Together, our approach, which is computationally effective, suggests new avenues for the design of shape-morphing and multistable metamaterials [15] as well as devices for robotics or deployable structures such as bellows [9,36].

System.—We consider collections of quadrilaterals connected in a square topology by hinges with zero torsional stiffness and finite stretchability (Fig. 1). For equally sized squares, such a system has a zero mode and is known as the rotating square mechanism [37]; this geometry underlies a large number of mechanical metamaterials [14,15,17,19,21,28,32,38]. Generalizations, including to regular tilings of alternatively sized squares, rectangles, or 3D, are well known [19,28,39,40]. The condition for such collections of quadrilaterals to form a mechanism are simple. For definiteness, we focus on 3×3 tilings of quadrilaterals [Fig. 1(a)]. We can consider such tilings as
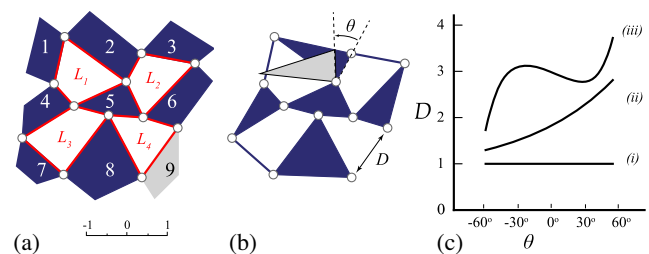

FIG. 1. (a) Full unit consisting of nine rigid quadrilaterals (1–9), connected by 12 flexible hinges $\{x_{12}, x_{23}, \ldots\}$ (circles). This unit can also be seen as four connected four-bar linkages L_i. (b) Diluted unit. (c) Depending on the design of quadrilaterals (1–8), the characteristic motion of the diluted unit, $D(\theta)$, can be (nearly) constant *(i)*, a monotonic function *(ii)*, or a nonmonotonic function *(iii)*.

collections of connected four-bar linkages L_i, and then express the relations between their (inner) angles by mappings M_i. It can be shown that quadrilateral tilings can only form a mechanism if all four-bar linkages (voids) form parallelograms, as these are associated with linear mappings M_i [41]. In contrast, for generic quadrilaterals the mappings M_i are nonlinear, and tilings of 3×3 (or larger) generic quadrilaterals do not possess a zero energy motion [38,41,42] [Fig. 1(a)].

To make progress, we focus on a diluted unit, obtained by removing quadrilateral 9, which yields a *mechanism* with a freely hinging, zero energy, finite amplitude mode [38,42] [Fig. 1(b)]. To characterize this mechanism, we remove all extraneous information, and replace the corner quadrilaterials with rigid bars [Fig. 1(b)]. The geometry of this mechanism is specified by the coordinates of the 12 links $\{x_{12}, x_{23}, \ldots\} =: X$, which span a 24-dimensional design space. We control the free motion of this mechanism by θ, the deviation of $\angle$ from its initial value, and characterize the diluted unit by $D := |x_{89} - x_{69}|$ as a function of θ [Fig. 1(b)]. Experimentally, stretching or compressing two points on the systems, or compressing the points between parallel plates actuates the soft mode of the system that we describe here. The function $D(\theta)$ acts as a proxy for the mechanics of a full 3×3 unit consisting of flexible elements: if $D(\theta)$ is a constant, reinserting a ninth quad of appropriate dimensions yields a full 3×3 unit with a zero mode [42,43] [Fig. 1(c)(i)]. For nearly constant $D(\theta)$, reinserting the ninth quadrilateral would lead to a system with a large amplitude motion with a very low energy: a *pseudo-mechanism*. For generic quadrilaterals $D(\theta)$ is a nonlinear function [Fig. 1(c)(ii–iii)], and inserting the ninth quadrilateral yields a more complex energy landscape. The design problem is thus to obtain coordinates $\{x_{12}, x_{23}, \ldots\}$ so that $D(\theta)$ closely matches a target function $D_t(\theta)$.

Design by particle swarm optimization.—We define a cost function f based on the normalized Euclidean distance between $D(\theta)$ and $D_t(\theta)$, combined with discrete constraints to avoid nonfitting quadrilaterals, overlapping quadrilaterals, and designs where the quadrilateral sizes differ too much (see Supplemental Material [44]). Exploring this design space requires an algorithm that does not easily get stuck in shallow minima, as purely gradient based methods would. Evolutionary algorithms are eminently suited for this, and we choose here to use particle swarm optimization (PSO) due to its simplicity and ease of tuning. This method employs an ensemble (swarm) of particles—each representing a particular design—and is known to allow one to identify deep minima in a rugged landscape [45–51]. While we note that our approach remains valid for larger structures, the computational time grows exponentially in the size of the structure and we focus here on 3×3 structures. The PSO algorithm keeps track of the best position discovered by each particle up to

generation (iteration) k, $\mathbf{xb}_i^k$, and by the best position discovered by all the particles—the swarm—$\mathbf{xs}^k$. We seed an initial population of randomly distributed particles with random velocities. During the search, each particle is attracted towards a stochastic mix of $\mathbf{xb}_i^k$ and $\mathbf{xs}^k$:

$$\mathbf{v}_i^{k+1} = w\mathbf{v}_i^k + c_1 \mathbf{r}_i^1 \cdot (\mathbf{xb}_i^k - \mathbf{x}_i^k) + c_2 \mathbf{r}_i^2 \cdot (\mathbf{xs}^k - \mathbf{x}_i^k), \quad (1)$$

$$\mathbf{x}_i^{k+1} = \mathbf{x}_i^k + \mathbf{v}_i^{k+1}, \quad (2)$$

where $\mathbf{r}_i^1$ and $\mathbf{r}_i^2$ are random vectors whose elements are uniformly distributed between 0 and 1, and the so-called inertia (w), cognition (c_1), and social (c_2) hyperparameters must be chosen to optimize convergence. For our specific design problem, the position $\mathbf{x}_i$ and velocity $\mathbf{v}_i$ of particle i are both 24-dimensional vectors, and we have verified by hyperparameter optimization that the algorithm yields good results for $w = 0.25$, $c_1 \geq 0.0$, $c_2 \geq 1.75$ and $c_1 + c_2 \leq 3.50$ (see Supplemental Material [44]). For each target function, we run 3000 runs for each of the 36 pairs of parameter values that satisfy $c_1 = 0, 0.25, 0.5, \ldots, 1.75$, $c_2 = 1.75, 2, 2.25, \ldots, 3.5$, and $c_1 + c_2 \leq 3.5$, leading to a total of 1.18×10^5 runs. For details, see Supplemental Material [44].

Generic flexible unit cells.—We first focus on designing diluted units for which $D(\theta)$ is close to a constant. We set the target curve $D_{t1}(\theta) = 1$ and deploy PSO to obtain designs with low values of f. We find a large number of designs for which f is very small, so that $D(\theta)$ is close to a constant (Fig. 2). We quantify the geometry of these solutions through an order-parameter s which measures the proximity of the four internal four-bar linkages to parallelogram linkages. We define s_i for the ith linkage as

$$s_i^2 = \frac{(a_i^1 - a_i^3)^2 + (a_i^2 - a_i^4)^2}{\sqrt{(a_i^1)^2 + (a_i^2)^2 + (a_i^3)^2 + (a_i^4)^2}}, \quad (3)$$

where a_i^j are the bar lengths $j = 1, \ldots, 4$ of linkage i, and define s as

$$s = \sqrt{\sum_{i=1}^{4} s_i^2}. \quad (4)$$

While our algorithm finds some solutions with small s, i.e., close to the true mechanism limit where all linkages are parallelograms [Fig. 2(a)], the vast majority of solutions with low f have significantly larger values of s [Figs. 2(b) and 2(c)]. Notwithstanding this strong deviation from true mechanisms, the peak deviation between $D(\theta)$ and $D_t(\theta)$ can be as small as 4×10^{-4} [Figs. 2(d)–2(f)].

We show a scatter plot of f versus s, and the individual distributions of f and s—which are only weakly correlated—in Figs. 2(g)–2(i). These plots reveal that the
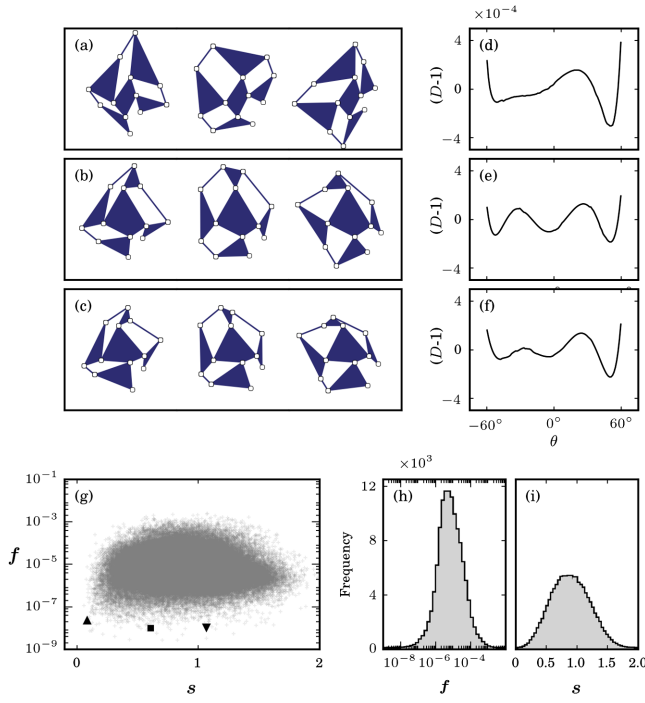
FIG. 2. (a)–(c) Three examples of diluted units for which $D(\theta)$ is nearly constant and equal to 1, for $\theta \in [-60°, 60°]$, for $[f, s] = [2.26 \times 10^{-8}, 0.084]$ (a); $[9.88 \times 10^{-9}, 0.611]$ (b); and $[1.04 \times 10^{-8}, 1.06]$ (c). The three snapshots in each panel correspond to $\theta = -60°, 0°$, and $60°$. (d)–(f) Corresponding plots of $D - 1$ vs θ; notice the scale. (g) Scatter plot of f vs s, where uptriangle, square, and downtriangle symbols indicate the parameter values shown in (a)–(c), respectively. (h),(i) Distributions of f and s.

distribution of f is log normal, with s normally distributed with the center at $s \approx 1$, corresponding to designs that are very far away from strict mechanisms ($s = 0$). Hence, pseudo-mechanisms with anomalously low functional deviations from true mechanisms are widespread, and

occur in regions of design space that are far away from true mechanisms.

Our findings suggest a complex organization of the design space. To gain insight into this structure, we have explored whether the value of f increases if a certain solution x_0 is randomly perturbed. Specifically, we generate 1000 random 24-dimensional vectors dx with each entry uniformly distributed between -1 and 1, and then calculate $f(x_0 + \varepsilon dx)$ for a range of ε. For the deep solution, where $[f_0, s] = [9.88 \times 10^{-9}, 0.61]$, we find that all $f > f_0$, consistent with the idea that these solutions are local minima (see Supplemental Material [44]). In contrast, for solutions with much larger values of f we find a small but finite probability that $f < f_0$ for small perturbations ($\varepsilon = 10^{-3}$) but not for larger perturbations of order $\varepsilon = 10^{-2}$. We suggest that these solutions perhaps are close to a shallow local minimum, and note that PSO is not guaranteed to find local minima with high accuracy (for details, see Supplemental Material [44]).

Multistable unit cells.—The ease with which we can find pseudo-mechanisms prompts the question if it is similarly easy to generate designs for other target functions. For systems with flexible hinges, inserting a ninth quad with dimension D' provides the blueprint for a unit with low energy states for $D(\theta) = D'$, so that nonmonotonic $D(\theta)$ lead to multistable structures. We have investigated four families of target function: $D_{1,t} = 1 + \alpha\theta$, $D_{2,t} = 1 + \alpha\sin(2\theta + \pi/2)$, $D_{3,t} = 1 + \alpha\sin(3\theta + \pi/2)$, and $D_{4,t} = 1 + \alpha\sin(4\theta)$ for a range of values of α between $-1/2$ and $1/2$ [52]. Here we focus on the designs for $D_{2,t}$ and $D_{4,t}$, as these form the basis for bistable and tristable units.

We show scatter plots of f vs s for $D_{2,t}$ and $D_{4,t}$ in Fig. 3, for $\alpha = 0.5$. We observe a large cloud of solutions, and note that the typical values of f for curves with more extrema are somewhat larger than those for $D_t = 1$. Examples of
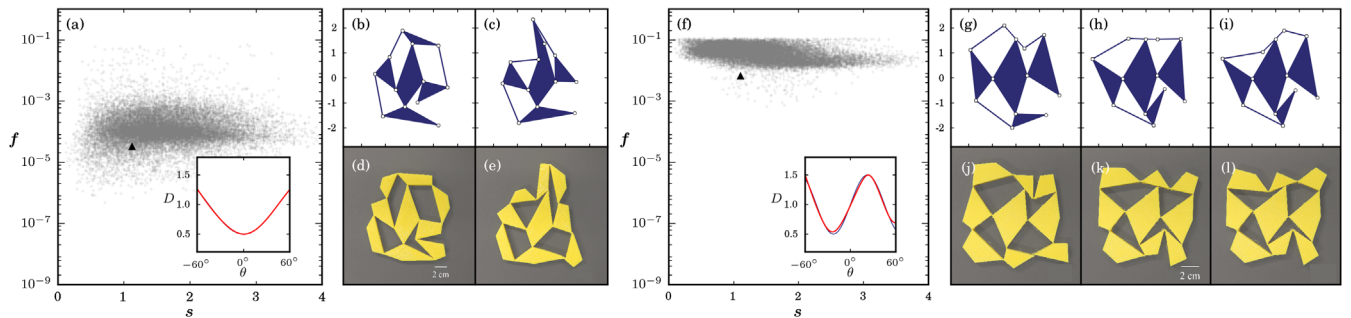

FIG. 3. (a) Scatter plot [18000 points] of f and s for the target function $D_t(\theta) = 1 + 0.5\sin(2\theta + \pi/2)$. Inset: The target and realized $D(\theta)$ for $f = 3.2 \times 10^{-5}, s = 1.12$ (triangle in panel (a)) are virtually indistinguishable. (b,c) Corresponding pruned unit for $\theta = \pm 60°$, where $D \approx 1$ (d,e) Corresponding 3D printed flexible bistable unit in both its stable states. (f) Scatter plot [18000 points] of f and s for a target function $D_t(\theta) = 1 + 0.5\sin(4\theta)$. Inset: The target and realized $D(\theta)$ for $f = 6.7 \times 10^{-3}, s = 1.10$ (triangle in panel (g)) are virtually indistinguishable. (g–i) Corresponding pruned unit for $\theta = -45°, 0°, 45°$, where $D \approx 1$. (j–l) 3D printed tristable unit in all three stable states.

designs of diluted units that closely satisfy the target curves are shown in Fig. 3.

We experimentally realized full units based on the designs shown in Figs. 3(b) and 3(g) by adding a ninth quad of appropriate length and then 3D printing these units with flexible material (filaflex). The out-of-plane thickness of these samples is 10 mm and the connecting hinges have a minimum thickness of ≈ 0.5 mm. Despite the finite flexibility of all quads, and the finite but small bending stiffness of their hinges, we observe that these samples are indeed bistable and tristable respectively, with their stable configurations close to the expected configurations [Figs. 3(d), 3(e) and 3(j)–3(l)].

Complex tilings.—Finally, we briefly outline how we can connect complex 3×3 units into larger systems. Each PM can be augmented by replacing the outer bars by triangles [Figs. 4(a) and 4(b)]. The outer tips of this unit form a quadrilateral, and as any quadrilateral can be tiled in a pattern where adjacent quadrilaterals are rotated by 180°, larger PMs can readily be designed by connecting these units [Fig. 4(c)]. One can similarly augment multistable unit cells, and for a tiling of general augmenting triangles one expects stable collective states only when all units are in the same configuration, as the "gap" distance between tips of triangles generally differs in different minima. However, the augmenting triangles can be chosen such that this gap has the same length in each stable state [Figs. 4(d) and 4(e)]. Connecting such augmented units in a tiling yields a design with energy minima when each individual unit is in its stable state, leading to a number of stable states which grows exponentially with system size [Figs. 4(f)–4(i)].

Summary and outlook.—We have presented a novel strategy for the design of metamaterial architectures, based on pseudo-mechanisms which can have a geometric structure which is surprisingly far removed from that of strict mechanisms. As similar pseudo-mechanisms can be observed in 2D origami, where PMs allow to circumvent the difficult design of rigidly folding mechanisms [11,12,33,35], we speculate that pseudo-mechanisms are generic and relevant for a wide classes of structures, including networks of hinged bars [22] and (3D) origami [20]. Moreover, the ease of designing multistable structures in a hierarchical fashion—coupling complex units in tilings—suggests one generalize this approach to other classes also.

Extensions of our work include the design of larger nonperiodic collections of quadrilaterals that form pseudo-mechanisms. Conceptually, the step from a 2×3 mechanism to a 3×3 pseudo-mechanism might be similar to that from a 3×3 to a 3×4 pseudo-mechanism, but it is an open question how the design space evolves for increasingly large systems. A further intriguing possibility arises for, e.g., bellows: while the volume of a polyhedron cannot change as it flexes, pseudo-mechanisms may in practice work equally well [36]. Moreover, we wonder whether pseudo-mechanisms can mimic an equivalent of the topological polarization, edge modes and corner modes observed in topologically nontrivial mechanical metamaterials that are based on true mechanisms [23–26]. Finally, our designs space is only of moderate dimensions, and obtaining nontrivial designs is computationally relatively cheap. This makes our designs eminently suited to test whether machine learning techniques would be suitable to, first, be trained to distinguish "good" from "bad" pseudo-mechanisms, second, to detect and classify multistable designs, and third, be used to speed up the design of such structures [53,54].
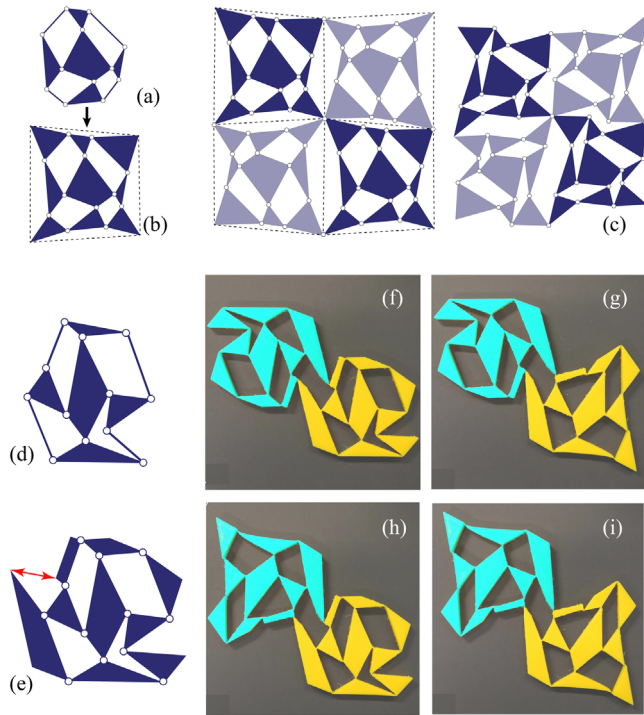

FIG. 4.   (a),(b) Design of a PM augmented by replacing the outer bars by triangles. (c) Staggered tiling of such PM has a soft hinging mode. (d) Bistable design. (e) Augmented design where gap distance (red arrow) has the same length in both stable states. (f)–(i) Two connected bistable 3D printed unit cells (green, yellow) can be snapped between four different stable states (false green color added for visibility).

[1] S. Alexander, Phys. Rep. **296,** 65 (1998).

[2] W. G. Ellenbroek, Z. Zeravcic, W. van Saarloos, and M. van Hecke, Europhys. Lett. **87,** 34004 (2009).

[3] W. G. Ellenbroek, V. F. Hagh, A. Kumar, M. F. Thorpe, and M. van Hecke, Phys. Rev. Lett. **114,** 135501 (2015).

[4] C. P. Goodrich, A. J. Liu, and S. R. Nagel, Phys. Rev. Lett. **114,** 225501 (2015).

[5] J. W. Rocks, N. Pashine, I. Bischofberger, C. P. Goodrich, A. J. Liu, and S. R. Nagel, Proc. Natl. Acad. Sci. U.S.A. **114,** 2520 (2017).

[6] A. J. Liu and S. R. Nagel, Annu. Rev. Condens. Matter Phys. **1,** 347 (2010).

[7] M. van Hecke, J. Phys. Condens. Matter **22,** 033101 (2010).

[8] C. Detweiler, M. Vona, Y. Yoon, S.-K. Yun, and D. Rus, IEEE Robot. Autom. Mag. **14,** 45 (2007).

[9] D. Rus and M. T. Tolley, Nature (London) **521,** 467 (2015).

[10] J. L. Silverberg *et al.*, Science **345,** 647 (2014).

[11] L. H. Dudte, E. Vouga, T. Tachi, and L. Mahadevan, Nat. Mater. **15,** 583 (2016).

[12] M. Stern, M. B. Pinson, and A. Murugan, Phys. Rev. X **7,** 041070 (2017).

[13] A. S. Meeussen, E. C. Oğuz, Y. Shokef, and M van Hecke, Nat. Phys. **16,** 307 (2020).

[14] C. Coulais, C. Kettenis, and M. van Hecke, Nat. Phys. **14,** 40 (2018).

[15] K. Bertoldi, V. Vitelli, J. Christensen, and M. van Hecke, Nat. Rev. Mater. **2,** 17066 (2017).

[16] R. S. Lakes, Science **235,** 1038 (1987).

[17] T. Mullin, S. Deschanel, K. Bertoldi, and M. C. Boyce, Phys. Rev. Lett. **99,** 084301 (2007).

[18] D. R. Reid *et al.*, Proc. Natl. Acad. Sci. U.S.A. **115,** E1384 (2018).

[19] C. Coulais, E. Teomy, K. de Reus, Y. Shokef, and M. van Hecke, Nature (London) **535,** 529 (2016).

[20] J. T. B. Overvelde, J. C. Weaver, C. Hoberman, and K. Bertoldi, Nature (London) **541,** 347 (2017).

[21] P. Celli *et al.*, Soft Matter **14,** 9744 (2018).

[22] J. Z. Kim, Z. X. Lu, S. H. Strogatz, and D. S Bassett, Nat. Phys. **15,** 714 (2019).

[23] J. Paulose, B. G. -g. Chen, and V. Vitelli, Nat. Phys. **11,** 153 (2015).

[24] B. G. -g. Chen, B. Liu, A. A. Evans, J. Paulose, I. Cohen, V. Vitelli, and C. D. Santangelo, Phys. Rev. Lett. **116,** 135501 (2016).

[25] D. Z. Rocklin, S. Zhou, K. Sun, and X. Mao, Nat. Commun. **8,** 14201 (2017).

[26] M. Serra-Garcia *et al.*, Nature (London) **555,** 342 (2018).

[27] A. Rafsanjani and D. Pasini, Extr. Mech. Lett. **9,** 291 (2016).

[28] B. Florijn, C. Coulais, and M. van Hecke, Phys. Rev. Lett. **113,** 175503 (2014).

[29] S. R. Waitukaitis, R. Menaut, B. G. -g. Chen, and M. van Hecke, Phys. Rev. Lett. **114,** 055503 (2015).

[30] E. T. Filipov, T. Tachi, and G. H. Paulino, Proc. Natl. Acad. Sci. U.S.A. **112,** 12321 (2015).

[31] E. T. Filipov, K. Liu, T. Tachi, M. Schenk, and G. H. Paulino, Int. J. Solid Struct. **124,** 26 (2017).

[32] C. Coulais, A. Sabbadini, F. Vink, and M. van Hecke, Nature (London) **561,** 512 (2018).

[33] M. Stern, V. Jayaram, and A. Murugan, Nat. Commun. **9,** 4303 (2018).

[34] S. H. Chen and L. Mahadevan, Proc. Natl. Acad. Sci. U.S.A. **116,** 8119 (2019).

[35] P. Dieleman, N. Vasmel, S. Waitukaitis, and M. van Hecke, Nat. Phys. **16,** 63 (2020).

[36] I. K. Sabitov, Discrete Comput. Geom. **20,** 405 (1998).

[37] J. N. Grima and K. E. Evans J. Mater. Sci. Lett. **19,** 1563 (2000).

[38] L. A. Lubbers and M. van Hecke, Phys. Rev. E **100,** 021001 (R) (2019).

[39] D. Rayneau-Kirkhope, C. Zhang, L. Theran, and M. A. Dias, Proc. R. Soc. A **474,** 20170753 (2018).

[40] Y. Tang *et al.*, Adv. Mater. **27,** 7181 (2015).

[41] Y. Yang and Z. You, J. Mech. Rob. **10,** 021001 (2018).

[42] C. R. Calladine, Int. J. Solid Struct. **14,** 161 (1978).

[43] Consistent with Maxwell-Calladine counting, such a mechanism possesses an associated state of self-stress [42].

[44] See Supplemental Material at http://link.aps.org/supplemental/10.1103/PhysRevLett.126.248002 for further details.

[45] J. Kennedy and R. Eberhart, Proc. IEEE Int. Conf. Neural Networks **4,** 1942 (1995).

[46] R. Poli, J. Kennedy, and T. Blackwell, Swarm Intell. **1,** 33 (2007).

[47] R. C. Eberhart and Y. H. Shi, IEEE Trans. Evol. Comput. **8,** 201 (2004).

[48] A. Chatterjee and P. Siarry, Computers and Operations Research **33,** 859 (2006).

[49] A. Nickabadi, M. M. Ebadzadeh, and R. Safabakhsh, Appl. Soft Comput. **11,** 3658 (2011).

[50] M. Pant, R. Thangaraj, and A. Abraham, Found. Comput. Intell. **3,** 101 (2009).

[51] A. L. Gutierrez, M. Lanza, I. Barriuso, L. Valle, M. Domingo, J. R. Perez, and J. Basterrechea, in *Proceedings of the 5th European Conference on Antennas and Propagation (EUCAP 2011)* (Springer, Rome, 2011), Vol. 5, p. 965.

[52] N. Singh, Strategies for mechanical metamaterial design, Ph.D. thesis, Leiden University, The Netherlands, 2019, http://hdl.handle.net/1887/71234.

[53] P. Z. Hanakata, E. D. Cubuk, D. K. Campbell, and H. S. Park, Phys. Rev. Lett. **121,** 255304 (2018).

[54] M. A. Bessa, P. Glowacki, and M. Houlder, Adv. Mater. **31,** 1904845 (2019).